DIRECT NUMERICAL SIMULATION OF MAGNETOHYDRODYNAMIC TURBULENT CHANNEL FLOWS

Myoungkyu Lee
Department of Mechanical Engineering
University of Houston
4226 Martin Luther King Blvd, Houston, TX 77204, USA
leemk@uh.edu

ABSTRACT

In this study, we conduct direct numerical simulations of magnetohydrodynamic turbulent channel flows, employing an inductionless assumption that keeps the magnetic fields constant due to low magnetic Reynolds number assumptions. We utilize pseudospectral methods alongside high-order basis splines for these simulations. Our analysis focuses on the influence of magnetic fields at a Reynolds number (*Re*) up to 20,000, examining the effects of various magnetic strengths quantified by Hartmann numbers (Ha). We explore changes in flow structure, Reynolds stress components, spectral densities, and budget equations for Reynolds normal stresses.

The results demonstrate that increasing Ha significantly alters flow behavior by reducing turbulence and promoting re-laminarization. Spectral analysis using polar-logarithmic coordinates indicates that higher Ha values suppress large-scale motions while emphasizing streamwise elongated motions. Analysis of the budget equations shows that while viscous transport and dissipation remain consistent across different Ha values, turbulent transport and production terms vary significantly. The magnetic field's contribution to the budget terms is nearly negligible. The decrease in production is identified as the primary mechanism by which magnetic fields suppress turbulence in these magnetohydrodynamic channel flows.

INTRODUCTION

While research on turbulent flows has extensively contributed to our understanding, our grasp of this complex phenomenon remains incomplete, especially when these flows interact with other physical processes like heat transfer or chemical reactions. Such interactions are exemplified in the domain of magnetohydrodynamics (MHD), where electrically conducting fluids engage with electromagnetic fields. Although MHD turbulence might not be evident in daily experiences, it is crucial in fields such as astrophysics, geophysics, and various engineering applications, significantly impacting our way of life (Biskamp, 2003; Davidson, 2015; Al-Habahbeh *et al.*, 2016).

A critical application of MHD wall-bounded turbulence is in nuclear fusion reactors, where fusion energy is seen as the next frontier in energy production, offering substantial benefits in terms of fuel reserves, safety, and environmental impact (FESAC). However, this area faces significant technological challenges. For instance, liquid metals, which have high thermal diffusivity and low viscosity, must be managed within insulated conduits under strong magnetic fields (Federici *et al.*, 2019; Smolentsev, 2021). Here, the Reynolds number (*Re*) is typically around 10^5, and the Hartmann number (Ha), which measures the strength of electromagnetic versus viscous forces, is on the order of 10^4. Such conditions lead to MHD pressure drops due to Lorenz forces opposing the flow, creating challenges in maintaining high flow rates essential for optimizing the efficiency of the liquid metal blanket within the constraints of structural strength (Abdou *et al.*, 2015; Mistrangelo & Bühler, 2017; Mistrangelo *et al.*, 2021).

Previous studies have illuminated various aspects of MHD turbulence. For example, Zikanov & Thess (1998) demonstrated how strong magnetic fields transform fully developed homogeneous isotropic turbulence into two-dimensional turbulence. Further, studies by Lee & Choi (2001); Satake *et al.* (2006) involved direct numerical simulations (DNS) of MHD channel flows under uniform magnetic fields. Lee & Choi (2001) noted that wall-normal magnetic fields are more effective than streamwise or spanwise fields in reducing turbulent fluctuations. Moreover, research by Satake *et al.* (2006); Boeck *et al.* (2007); Pothérat & Kornet (2015) showed that increasing Ha leads to a reduction in large-scale structures in MHD turbulent channel flows. On the other hand, Krasnov *et al.* (2008) observed that magnetic fields aligned in the spanwise direction can reduce drag, contrasting with results from flows under wall-normal magnetic fields. Despite extensive research, the lifecycle of turbulence in MHD wall-bounded flows—from production to dissipation—remains unclear.

This study serves as preliminary work aimed at understanding the lifecycle of turbulence in MHD wall-bounded flows, focusing particularly on the fundamental impact of applied magnetic fields on electrically conductive flows at high *Re* and moderate Ha, and analyzing the spectral behavior of Reynolds stress and its evolution.

METHOD

In this study, we perform Direct Numerical Simulations (DNS) of incompressible magnetohydrodynamic wall-bounded turbulence (MHDWBT) within the canonical channel flow geometry. We made the assumption of a low magnetic Reynolds number, allowing us to disregard the alteration of magnetic fields caused by fluid motion.

The governing equations describing the velocity field, denoted as $\mathbf{u}$, in the presence of a constant magnetic field $\mathbf{B}$ for incompressible conductive flows can be found in Zikanov &

Thess (1998); Lee & Choi (2001); Satake *et al.* (2006).

For this study, we conduct DNS of incompressible magnetohydrodynamic wall-bounded turbulence (MHDWBT) in the canonical channel flow geometry. Based on the low magnetic Reynolds number assumption, we ignored the change of magnetic fields induced by fluid flows. The governing equations of the velocity field, $\mathbf{u}$ with a constant magnetic field, $\mathbf{B}$, of incompressible conductive flows are as described in Zikanov & Thess (1998); Lee & Choi (2001); Satake *et al.* (2006).

$$\nabla \cdot \mathbf{u} = 0 \tag{1a}$$

$$\frac{\partial \mathbf{u}}{\partial t} = -(\mathbf{u}\cdot\nabla)\mathbf{u} - \nabla p + \frac{Ha^2}{Re}(\mathbf{J}\times\mathbf{B}) + \nu\nabla^2\mathbf{u} \tag{1b}$$

Here $\mathbf{J}$, Re, and Ha are current density, Reynolds number, and Hartmann number, respectively. The density, half width of the channel and bulk velocity are fixed at unity for brevity, *i.e.* $Re = 1/\nu$, as is the magnetic field magnitude. Also, $Ha = 2|\mathbf{B}|\sqrt{\sigma/\nu}$ where σ is electric conductivity. Note that Ha^2/Re is Stuart number, $\mathscr{N}$. The relationship between $\mathbf{J}$ and $\mathbf{u}$ are obtained from Ohm's law and Gauss' law,

$$\mathbf{J} = -\nabla\phi + (\mathbf{u}\times\mathbf{B}), \quad \nabla^2\phi = \mathbf{B}\cdot(\nabla\times\mathbf{u}) = \mathbf{B}\cdot\omega \tag{2}$$

where ϕ is the electric potential. For computational efficiency, we employed the velocity-vorticity formulation, a method that has been utilized in numerous DNS studies of channel flows (Kim *et al.*, 1987). Our in-house simulation code, previously employed for DNS investigations of channel flows at a Reynolds number of approximately $Re_\tau \approx 5200$ (Lee & Moser, 2015), underwent necessary modifications. In the calculation of spatial derivatives, we applied the Fourier-Galerkin method in the streamwise and spanwise directions, while utilizing a seventh-order basis spline method in the wall-normal direction. Further details about our simulation code can be found in references Lee *et al.* (2013, 2014). To validate the modified simulation code, we conducted a comparison of statistics with identical simulation cases conducted by Satake *et al.* (2006).

Table 1. This is an example of a table.

Re	Re_τ^H	N_x	N_y	N_z
2857	182	1024	192	512
10000	544	1536	384	1024
20000	1000	2304	512	2048

In this study, we investigate the impact of constant magnetic fields applied in the wall-normal direction on turbulent flows at various combinations of Res and Has. Specifically, we selected three bulk Reynolds numbers: $Re = 2857$, $Re = 10000$, and $Re = 20000$, which correspond to friction Reynolds numbers Re_τ of 182, 544, and 1000, respectively, when $Ha = 0$. The computational grid size is detailed in Table 1. For each Re, we consider five different cases with Ha values of 1, 3, 10, 30, and 100. The simulations commence with velocity fields representing fully developed turbulent channel flows at $Ha = 0$. We gather statistical data after the initial transient state has subsided. To ensure the reliability of our results, we assess the convergence of statistics using total shear stress, and we find that the statistical error remains below 0.2% for all cases.

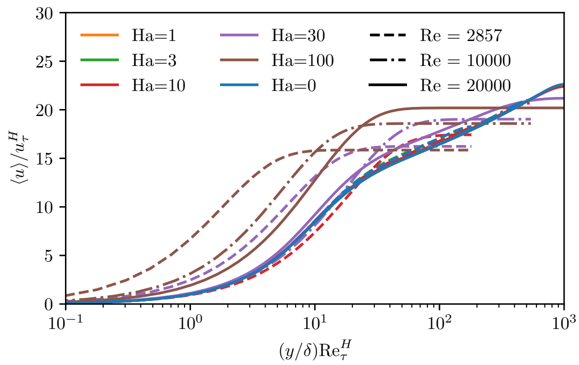

Figure 1. Mean velocity profiles

RESULTS

In this study, all statistical quantities and the wall-normal distance are normalized using their respective friction velocities and viscous length scales corresponding to each Re, in the absence of an applied magnetic field ($Ha = 0$).

Figure 1 presents the mean profiles of streamwise velocity for all simulation cases. Typically, the influence of increasing Ha begins in the channel's central region, where the gradient of the mean velocity becomes significantly flattened. In scenarios where Ha greatly exceeds Re, the mean velocity profile tends toward uniformity across almost the entire channel, except near the walls where it increases linearly with the wall-normal distance. Due to the expanded region of the flattened velocity profile, there is a requirement for a rapid velocity change near the walls. Consequently, this results in a higher mean velocity gradient at the walls in the presence of magnetic fields, leading to an increase in net skin friction. It is noteworthy that the characteristic behavior of the "logarithmic region," characterized by $y\partial_y\langle U\rangle = 0$, is absent in these cases, likely due to the relatively low Re and the significant impact of magnetic fields on the outer flow dynamics. When Ha is sufficiently high, the region where the mean velocity is constant expands even to the near-wall region, where the mean velocity linearly increases with y. Under such conditions, turbulence is completely suppressed, and the flow becomes laminar. This analytic description of the mean velocity for laminar flow is known as the Hartmann solution (Hartmann, 1937; Shercliff, 1953), which is invariant with respect to Re.

$$u(y) = \frac{Ha}{\tanh(Ha) - Ha}\left[\frac{\cosh(yHa)}{\cosh(Ha)} - 1\right] \tag{3}$$

The variations in figure 1 across different Res are due to different normalization factors.

Figure 2 illustrates the profiles of the non-zero components of Reynolds stress. Generally, high Ha significantly reduce turbulent fluctuations, suggesting a re-laminarization of the flow. At moderate Ha levels, magnetic fields effectively suppress turbulence in the outer flow regions. For example, in flows with $Ha = 30$ and $Re = 20000$, u'^2 is significantly reduced in the outer region, with only a slight reduction near the wall. The impact of the magnetic field is par-

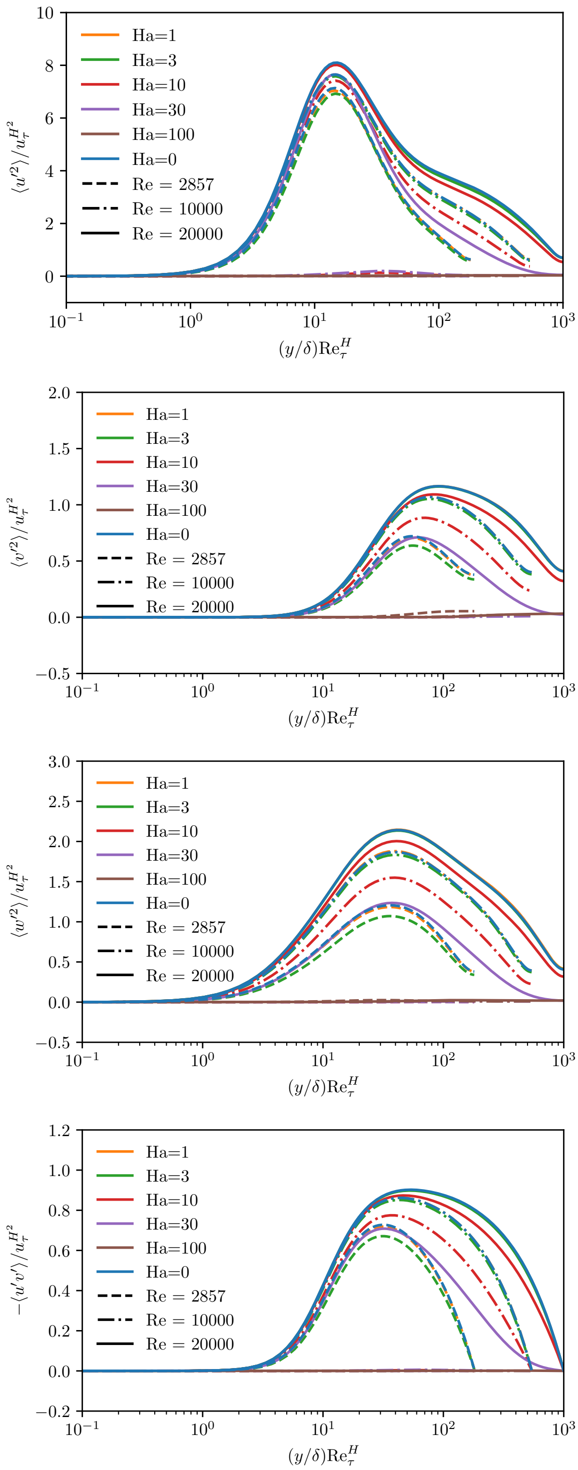

Figure 2. Reynolds stress profiles

ticularly pronounced on v'^2 and w'^2, enhancing anisotropy in the near-wall region as u'^2 remains relatively stronger until the flow re-laminarizes. Nonetheless, all components of Reynolds stress peak at the same location unless the flow is completely re-laminarized.

Furthermore, Reynolds shear stress shows a strong dependence on the strength of the magnetic fields. In channel flow geometry, the balance between mean shear stress, Reynolds shear stress, and magnetic stresses is required to maintain the total stress as a linear function of y. The observed changes in Reynolds stress suggest an increase in magnetic shear stress in the outer flow region, especially since the mean shear stress there is minimal. This finding aligns with observations by Satake *et al.* (2006) at low *Re*s.

Figure 3 shows the streamwise velocity at the wall-normal position where $\langle u'^2 \rangle$ peaks, specifically at $(y/\delta)\mathrm{Re}_\tau^H = 15$ for $Re = 20000$. In the absence of a magnetic field ($Ha = 0$), fine-scale structures are clustered yet exhibit fluctuations on a larger scale. Conversely, at $Ha = 30$, the small-scale structures are more organized and show minimal large-scale fluctuations, indicating that magnetic fields suppress large-scale motions. It is noted that at $Ha = 0$, large-scale structures in the near-wall region reflect those of the outer flow, as reported by Marusic *et al.* (2010); Lee & Moser (2019). With the suppression of large-scale motion in the outer flow, this near-wall imprint is diminished. A more detailed analysis using spectral densities could provide a clearer explanation.

Figures 4 present the two-dimensional spectral density of Reynolds normal stresses at their peak values, focusing on flows with $Re = 20000$, where large-scale contributions are most pronounced. Traditional k_x and k_z premultiplied two-dimensional spectra indicate that the contributions from large-scale motions are diminished, although the contributions at $k_x = 0$ or $k_z = 0$ remain significant. To address this, we employ polar-logarithmic coordinates as suggested by Lee & Moser (2019).

In this format, the two-dimensional spectral density $E(k_x, k_z)$ is transformed into rescaled spectral density $E^\#$ in polar-logarithmic coordinates, defined as follows:

$$E^\#(k_x^\#, k_z^\#) = \frac{k^2 E(k_x, k_z)}{\xi}, \tag{4a}$$

$$k_x^\# = \frac{\xi k_x}{k}, \quad k_z^\# = \frac{\xi k_z}{k}, \tag{4b}$$

$$k = \sqrt{k_x^2 + k_z^2}, \quad \xi = \ln\left(\frac{k}{k_\mathrm{ref}}\right). \tag{4c}$$

where k_ref is a reference wavenumber, set at $k_\mathrm{ref}^+ = 1/5000$ for this study. It is important to note that the integration of $E^\#$ over $k_x^\#$ and $k_z^\#$ is equivalent to the integration of E over k_x and k_z:

$$\langle u_i u_j \rangle = \iint E_{ij}(k_x, k_z) \mathrm{d}k_x \mathrm{d}k_z = \iint E_{ij}^\#(k_x^\#, k_z^\#) \mathrm{d}k_x^\# \mathrm{d}k_z^\# \tag{5}$$

In figures 4a and d, $E_{u'^2}^\#$ shows that energies are predominantly concentrated in streamwise elongated motions, with peaks at $\lambda^+ = 100$ and $k_x \approx 0$, reflecting the spacing between streaky structures observed in figure 3. The large-scale contribution is distinctly visible in figure 4a but absent in figure 4d. Interestingly, although the peak value in figure 4d for the small-scale region is stronger than that in figure 4a, the integrated value, $\langle u'^2 \rangle (y^+ = 15)$, is higher in the flow without a magnetic field ($Ha = 0$) than with $Ha = 30$. Figures 4b and e, which display $E_{v'^2}^\#$, show no significant contribution from large-scale motions beyond $\lambda^+ = 1000$ in either case. The overall spectral distribution of $\langle v'^2 \rangle (y = 91)$ is similar between different Ha levels, although the intensity is much reduced at $Ha = 30$. Finally, figures 4c and f illustrate the spectral density of $E_{w'^2}^\#$. In flows with $Ha = 30$, the contributions from large-scale motions are moderate, and the strength in the small-scale region is also weaker compared to the flow at $Ha = 0$.

Finally, we analyzed the budget equations for $\langle u'^2 \rangle$. Following the conventional definitions of each term as suggested by Mansour (1988) for flows with $Ha = 0$, we introduce an

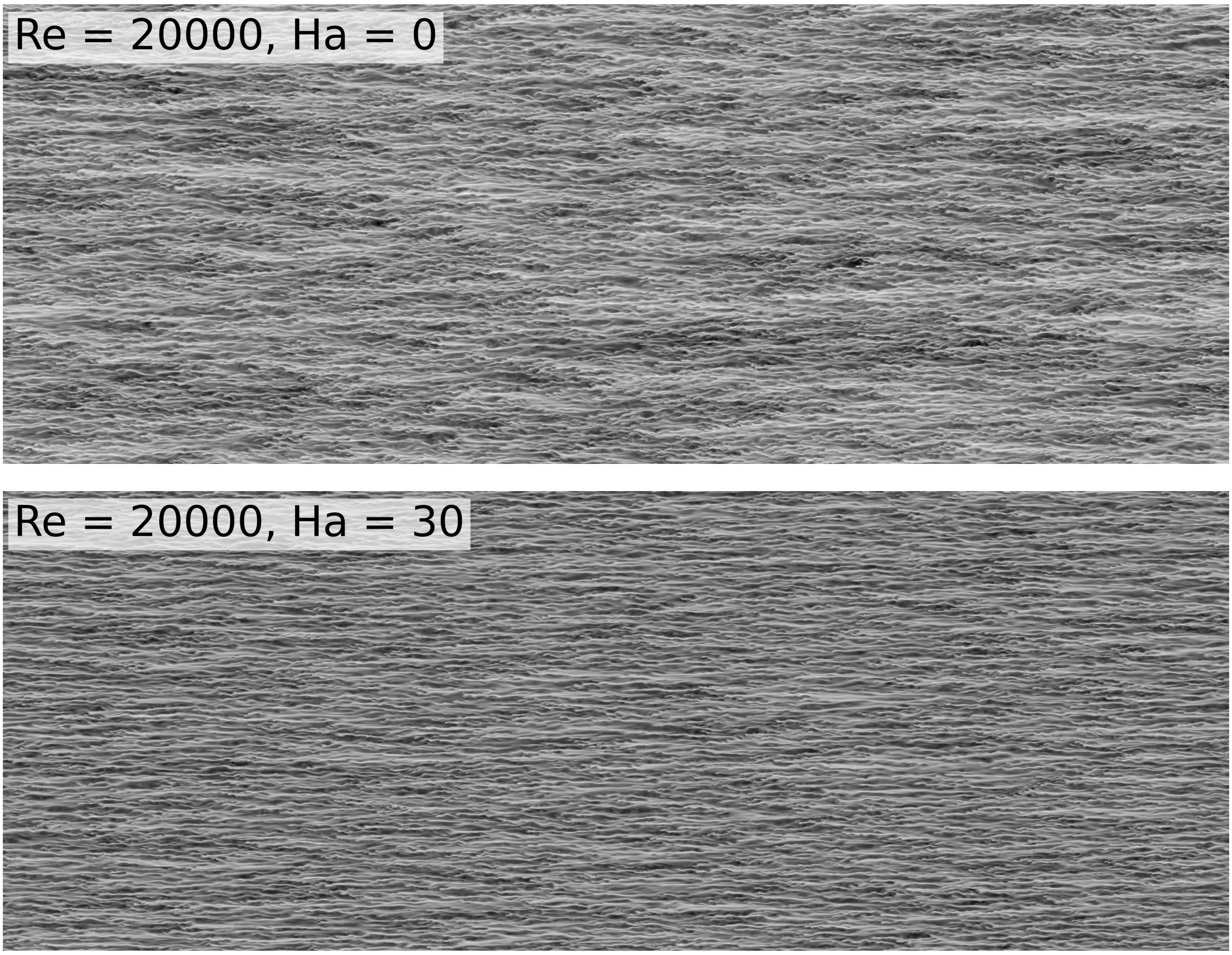

Figure 3. Streamwise velocity at where $\langle u'^2 \rangle$ is maximum

additional term to account for the effects of magnetic fields in these flows. Since a constant magnetic field is applied in the wall-normal direction, the resultant magnetic field term is expressed as follows:

$$M_{u'^2} = \frac{Ha^2}{Re} \left(2 \left\langle u' \frac{\partial \phi'}{\partial z} \right\rangle - 2\langle u'^2 \rangle \right) \tag{6}$$

The other terms are defined as follows: P - production, T - turbulent transport in the wall-normal direction, D - viscous transport in the wall-normal direction, Π - pressure strain, and ε - viscous dissipation. Figure 5 presents y-premultiplied budget terms for flows at $Re = 20000$ with $Ha = 0$ and $Ha = 30$.

In both cases, the viscous transport and dissipation show no noticeable difference. However, the turbulent transport terms differ in the outer-flow region; at $Ha = 0$, some energy is transported to the outer flows, whereas turbulent transport at $Ha = 30$ only reaches up to $y^+(= Re_\tau^H y/\delta) = 200$. Interestingly, the effect of $M_{u'^2}$ is almost negligible across the entire region. Based on the definition in (6), this suggests that $\langle u'\partial_z \phi' \rangle \approx \langle u'^2 \rangle$ and $\partial_z \phi' \approx u'$, though the implications of this remain unclear.

The production term shows the greatest influence of magnetic fields. P denotes the interaction between turbulent fluctuations and the mean-velocity gradient. In canonical channel flow geometry, P is defined as:

$$P = -\langle u'v' \rangle \frac{\partial \langle u \rangle}{\partial y} \tag{7}$$

As depicted in figure 1, applied magnetic fields effectively flatten the mean-velocity gradient. Moreover, as shown in figure 2d, the Reynolds shear stress, $\langle u'v' \rangle$, in the outer flow region decreases with increasing Ha. Consequently, the production of $\langle u'^2 \rangle$ in the outer flows decreases with Ha. This reduction also affects the inter-component energy transfer from $\langle u' \rangle$ to $\langle v'^2 \rangle$ and $\langle w'^2 \rangle$ in the outer flow region, leading to decreased values of these quantities with increasing Ha across all cases.

CONCLUSION

In this study, we present results from DNS of MHD wall-bounded turbulence, showing how magnetic fields suppress large-scale motions in the outer flows and modify turbulence structures near the wall. These findings are consistent with earlier research, including studies by Satake *et al.* (2006); Boeck *et al.* (2007). Notably, two-dimensional spectral density analysis indicates that magnetic fields intensify small-scale streaky motions in the near-wall flows.

Additionally, the direct impact of magnetic fields on turbulence, as depicted in the budget equations, appears minimal. This may be attributed to the simulations' assumption of

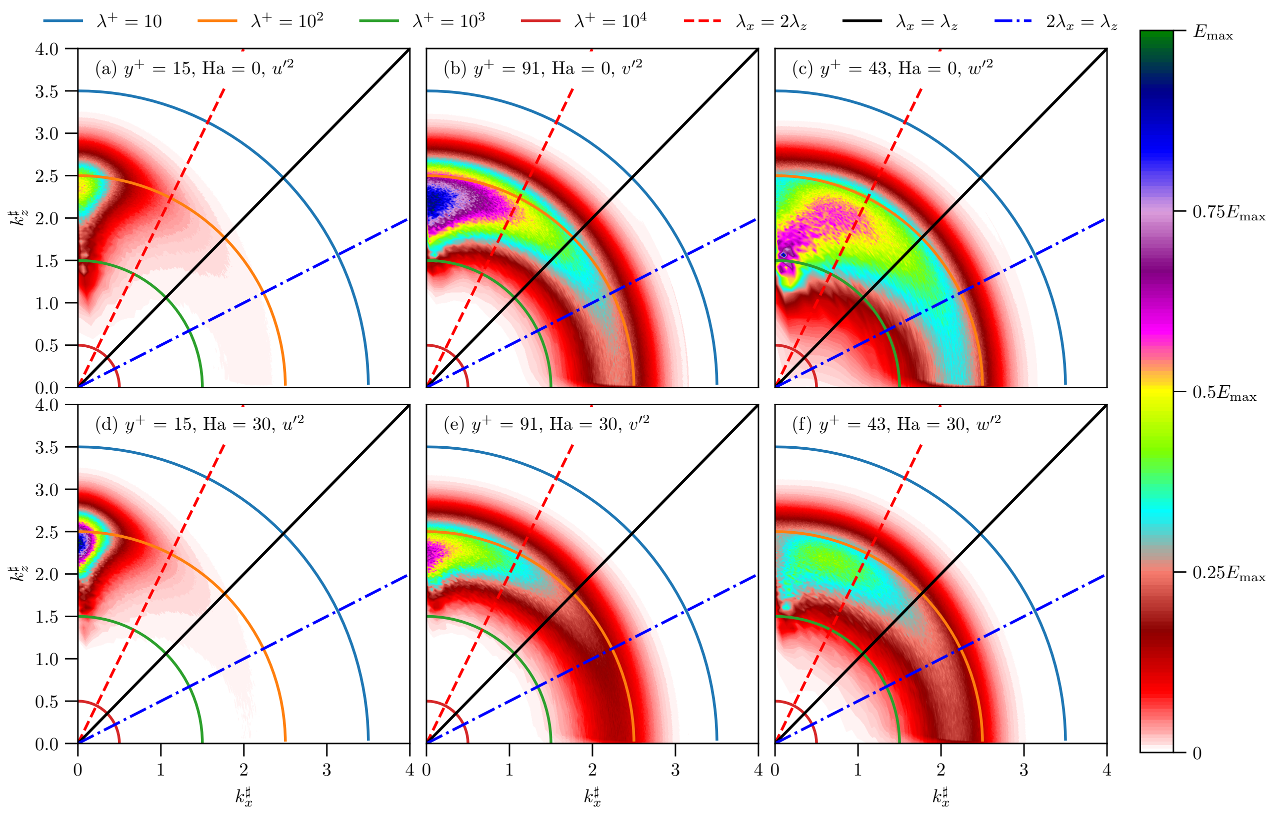

Figure 4. Streamwise velocity at where $\langle u'^2 \rangle$ is maximum

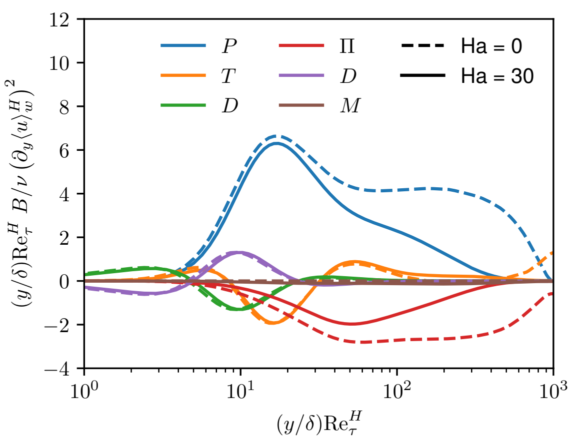

Figure 5. Budget terms

constant magnetic fields, which results in a linear interaction between the magnetic and velocity fields. However, in realistic scenarios, turbulent flows can induce fluctuations in the magnetic field, leading to nonlinear coupling between these fluctuations and flow turbulence. This implies that the influence of magnetic field fluctuations might be more critical than constant fields, potentially amplifying the effects of magnetic interactions on turbulence dynamics.

Lastly, this study serves as an initial exploration into the spectral analysis of budget equations in MHD channel flows. We observed an unexpected strengthening of $\langle u'^2 \rangle$ under magnetic fields in the spectral domain, suggesting that the spectral behavior of each term in the budget equation may differ, even though the integrated budget terms appear similar. This indicates that further detailed investigation is necessary to fully understand these dynamics.

ACKNOWLEDGEMENT

An award of computer time was provided by the Innovative and Novel Computational Impact on Theory and Experiment (INCITE) program. This research used resources of the Argonne Leadership Computing Facility, which is a DOE Office of Science User Facility supported under Contract DE-AC02-06CH11357.

REFERENCES

Abdou, M., Morley, N., Smolentsev, S., Ying, A., Malang, S., Rowcliffe, A. & Ulrickson, M. 2015 Blanket/first wall challenges and required R&D on the pathway to DEMO. *Fusion Engineering and Design* **100**.

Al-Habahbeh, O M, Al-Saqqa, M, Safi, M & Khater, T Abo 2016 Review of magnetohydrodynamic pump applications. *Alexandria Engineering Journal* **55**, 1347–1358.

Biskamp, D. 2003 *Magnetohydrodynamic Turbulence*. Cambridge University Press.

Boeck, Thomas, Krasnov, Dmitry & Zienicke, Egbert 2007 Numerical study of turbulent magnetohydrodynamic channel flow. *Journal of Fluid Mechanics* **572**, 179–188.

Davidson, Peter 2015 *Turbulence*. Oxford University Press.

Federici, G., Boccaccini, L., Cismondi, F., Gasparotto, M., Poitevin, Y. & Ricapito, I. 2019 An overview of the EU breeding blanket design strategy as an integral part of the DEMO design effort. *Fusion Engineering and Design* **141**, 30–42.

(FESAC), Fusion Energy Sciences Advisory Committee, Carter, Troy, Baalrud, Scott, Betti, Riccardo, Ellis, Tyler, Foster, John, Geddes, Cameron, Gleason, Arianna, Holland, Chistopher, Humrickhouse, Paul, Kessel, Charles, Lasa, Ane, Ma, Tammy, Maingi, Rajesh, Schaffner, David, Schmitz, Oliver, Shumlak, Uri, Snead, Lance, Solomon, Wayne, Trask, Erik, Waelbroeck, François, White, Anne & Rej, Ron 2020 Powering the Future: Fusion & Plasmas. *Tech. Rep.*.

Hartmann, J. 1937 Hg-Dynamics I. Theory of the Laminar Flow of an Electrically Conductive Liquid in a Homogeneous Magnetic Field. *Mathematisk-fysiske Meddelelser. XV, 6* .

Kim, J., Moin, P. & Moser, R. 1987 Turbulence statistics in fully developed channel flow at low reynolds number. *Journal of Fluid Mechanics* **177**, 133–166.

Krasnov, Dmitry, Zikanov, Oleg, Schumacher, Jörg & Boeck, Thomas 2008 Magnetohydrodynamic turbulence in a channel with spanwise magnetic field. *Physics of Fluids* **20**.

Lee, D. & Choi, H. 2001 Magnetohydrodynamic turbulent flow in a channel at low magnetic reynolds number. *Journal of Fluid Mechanics* **439**, 367–394.

Lee, M., Malaya, N. & Moser, R. 2013 Petascale direct numerical simulation of turbulent channel flow on up to 786k cores. ACM Press.

Lee, M. & Moser, R. 2015 Direct numerical simulation of turbulent channel flow up to $Re_\tau = 5200$. *Journal of Fluid Mechanics* **774**, 395–415.

Lee, M. & Moser, R. 2019 Spectral analysis of the budget equation in turbulent channel flows at high reynolds number. *Journal of Fluid Mechanics* **860**, 886–938.

Lee, M., Ulerich, R., Malaya, N. & Moser, R. 2014 Experiences from leadership computing in simulations of turbulent fluid flows. *Computing in Science and Engineering* **16**, 24–31.

Marusic, I., Mathis, R. & Hutchins, N. 2010 Predictive model for wall-bounded turbulent flow. *Science* **329**, 193–196.

Mistrangelo, Chiara & Bühler, Leo 2017 Magnetohydrodynamic flows in liquid metal blankets for fusion reactors. *PAMM · Proc. Appl. Math. Mech* **17**, 115–118.

Mistrangelo, C., Bühler, L., Smolentsev, S., Klüber, V., Maione, I. & Aubert, J. 2021 MHD flow in liquid metal blankets: Major design issues, MHD guidelines and numerical analysis. *Fusion Engineering and Design* **173**.

Pothérat, Alban & Kornet, Kacper 2015 The decay of wall-bounded MHD turbulence at low Rm. *Journal of Fluid Mechanics* **783**, 605–636.

Satake, S., Kunugi, T., Takase, K. & Ose, Y. 2006 Direct numerical simulation of turbulent channel flow under a uniform magnetic field for large-scale structures at high reynolds number. *Physics of Fluids* **18**, 125106.

Shercliff, J. A. 1953 Steady motion of conducting fluids in pipes under transverse magnetic fields. *Mathematical Proceedings of the Cambridge Philosophical Society* **49**, 136–144.

Smolentsev, S. 2021 Physical Background, Computations and Practical Issues of the Magnetohydrodynamic Pressure Drop in a Fusion Liquid Metal Blanket. *Fluids* **6** (3), 110.

Zikanov, O. & Thess, A. 1998 Direct numerical simulation of forced mhd turbulence at low magnetic reynolds number. *Journal of Fluid Mechanics* **358**, 299–333.